Published in Applied Optics 57, 16, 4707-4713, 2018
which should be used for any reference to this work

Rb vapor-cell clock demonstration with a frequency-doubled telecom laser

Nil Almat,* Matthieu Pellaton, William Moreno, Florian Gruet, Christoph Affolderbach, and Gaetano Mileti

Laboratoire Temps-Fréquence, Université de Neuchâtel, 2000 Neuchâtel, Switzerland
**Corresponding author: nil.almat@unine.ch*

We employ a recently developed laser system, based on a low-noise telecom laser emitting around 1.56 μm, to evaluate its impact on the performance of an Rb vapor-cell clock in a continuous-wave double-resonance scheme. The achieved short-term clock instability below $2.5 \cdot 10^{-13} \cdot \tau^{-1/2}$ demonstrates, for the first time, the suitability of a frequency-doubled telecom laser for this specific application. We measure and study quantitatively the impact of laser amplitude and frequency noises and of the ac Stark shift, which limit the clock frequency stability on short timescales. We also report on the detailed noise budgets and demonstrate experimentally that, under certain conditions, the short-term stability of the clock operated with the low-noise telecom laser is improved by a factor of three compared to clock operation using the direct 780-nm laser.

OCIS codes: (140.2020) Diode lasers; (140.3515) Lasers, frequency doubled; (300.6210) Spectroscopy, atomic; (300.6360) Spectroscopy, laser; (300.6370) Spectroscopy, microwave; (120.3940) Metrology.

1. INTRODUCTION

Since the first demonstration in 1989 [1], frequency-doubled laser diodes (LD) emitting in the telecom C-band at 1.56 μm and stabilized on rubidium (Rb) transitions around 780 nm have attracted a great interest for applications at both wavelengths, in the telecom C-band, and in applications requiring optical fields resonant with Rb transitions at 780 nm [2–5]. The need for optical telecommunications stimulated the development of reliable and reproducible optical sources with long lifetime and high spectral purity (i.e., single-mode operation, low noise, and narrow linewidth). Frequency doubling of these telecom lasers offers an interesting alternative to LDs emitting directly at the Rb wavelength (780 nm) for high-precision applications [6–8]. Here, we demonstrate for the first time the implementation of a similar laser system based on a frequency-doubled telecom laser in high-performance Rb vapor-cell atomic clocks [9,10] and present a quantitative analysis of the obtained clock stabilities.

One of the main issues in the atomic clock industry is the availability, reliability, reproducibility, and lifetime of LDs emitting around the atomic transition wavelengths. Hence, the well-established telecom lasers combined with the frequency-doubling technology provide a convenient solution in the development of reliable laser-pumped Rb vapor-cell clocks with long lifetimes. Besides, in Rb vapor-cell clocks, the laser is used for both optical pumping and optical detection of the clock signal [9,10]. Since the laser spectral properties play a crucial role in the clock performance, the requirements for the laser source are stringent for such applications [11]. The laser intensity and frequency fluctuations may impact the clock stability at all timescales, through different processes. In this study, we focus on short-term averaging times lying between 0.1 and 10 s. In these short timescales, the achievable clock performance is largely determined by the signal-to-noise ratio (S/N) of the resonance detection. The detection noise mainly originates from the intrinsic laser amplitude (AM) and frequency modulation (FM) noises. The laser FM noise contribution to the clock instability results from the FM-to-AM noise conversion [12,13] through the atomic absorption in the clock cell. The FM-to-AM noise conversion phenomenon depends strongly on the experimental conditions (laser frequency, cell temperature, etc.) and is usually one of the dominant limiting factors for short-term clock stability [14]. Thus, in order to reduce the optical detection noise contribution to short-term clock instability, low FM-noise lasers available in the telecom C-band become attractive candidates for their use in high-performance Rb vapor-cell clocks.

Previously, our group has developed compact laser systems based on LDs emitting directly at 780 nm and stabilized on Rb transitions for high-performance Rb clocks [15]. Using these in-house built laser systems based on 780-nm LDs, state-of-the-art short-term clock stability was demonstrated in

Ref. [14] for a clock operating in the continuous-wave double-resonance (CW-DR) scheme [14,16]. More recently, we have also developed a compact laser system based on a LD emitting at the telecom C-band that is frequency-doubled and stabilized on Rb transitions for CO_2 detection as reported in Ref. [17]. Then, we have evaluated in Ref. [18] the spectral characteristics of two frequency-doubled telecom lasers based on different chip technologies in view of their exploitation in high-performance Rb clocks. In particular, we have measured the laser intensity and frequency fluctuations and estimated their impacts on the clock performance compared to the laser systems based on 780-nm LDs [18]. In this present paper, we measure and evaluate quantitatively the impact of the laser spectral properties on the stability of a Rb vapor-cell clock.

In the following, we demonstrate a Rb vapor-cell clock operated in the CW-DR scheme and making use of a low-noise telecom laser that is frequency-doubled and stabilized on the Rb D_2 line. First, we report on the detailed analysis of the short-term clock instability budgets, then we present the clock instability measurements in comparison with those achieved with a laser head based on a LD emitting directly at 780 nm.

2. EXPERIMENTAL SETUP

Our experimental setup includes two main parts; the first one for laser frequency stabilization and the second one for Rb vapor-cell clock operation in a CW-DR scheme, as shown in Fig. 1. The laser light is transferred to the clock setup through a mechanically and thermally isolated 780-nm polarization-maintaining (PM) optical patch cord. We use two different laser systems. One of them is an in-house built laser head (LH) based on a distributed-feedback (DFB) LD emitting at 780 nm and comprising a dedicated frequency stabilization module integrated in its 0.63-dm^3 volume (more details on LH can be found in Ref. [15]). The other laser system is based on a fiber-pigtailed 1.56-μm laser diode (1.56 μm-LD). The output of the 1.56 μm-LD is frequency doubled through a second harmonic generation (SHG) unit based on a commercial 34-mm-long periodically poled lithium niobate waveguide as in Ref. [18], then separated in two equal parts by a fused coupler. One part is used to stabilize the laser frequency through an evacuated Rb cell situated in a frequency reference unit (FRU) [18] in the Doppler-free scheme. This FRU is very

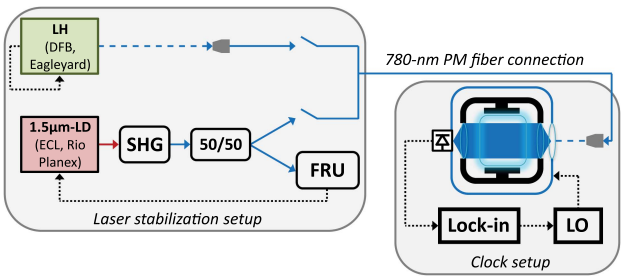

Fig. 1. Schematics of the experimental setup. The LH includes its own dedicated frequency stabilization module, while the 1.5 μm-LD is frequency stabilized using the separate FRU. Blue dashed line: free-space optical path. Blue full line: 780-nm PM optical patch cord. Red full line: 1.56-μm PM optical patch cord. Black dotted line: electrical signal.

similar to the one integrated in the LH, and the two evacuated Rb cells are identical. The light from the second output of the fused coupler is sent for the CW-DR experiments.

The CW-DR clock setup mainly consists of the physics package (PP), the local oscillator (LO) used to generate the microwave radiation, and the lock-in amplifier for synchronous detection. The PP is formed by a 25-mm glass cell filled with Rb and buffer gases, which is held in a magnetron-type microwave cavity [19] resonant with the Rb ground-state hyperfine splitting frequency ($\nu_{Rb} = 6'834'682'611$ Hz). The cell-cavity assembly is surrounded by a solenoid inducing a static magnetic field (C-field) to lift the degeneracy of the hyperfine energy levels, and the whole ensemble is enclosed in a mu-metal shielding and thermal isolation layers. A beam expander in front of the PP ensures the illumination of a large portion of the cell volume, with the laser beam diameter approximately equal to the cell diameter. After passing through the cell, the laser beam is focused on a photodetector. In the CW-DR scheme, the microwave radiation serving to interrogate the Rb atoms is applied to the Rb cell in the cavity simultaneously with the laser light. The double resonance (DR) signal is optically detected by the light transmitted through the cell as a function of the microwave frequency. The central frequency of the DR signal, the so-called clock frequency, corresponding to the Rb ground-state hyperfine splitting frequency for the given cell, is mainly shifted from the unperturbed Rb frequency due to the buffer gas pressure. The frequency of the microwave radiation injected in the cavity is frequency-modulated, and the optically detected signal is then demodulated using the lock-in amplifier to generate an error signal. The correction signal is subsequently fed back to the microwave synthesizer to stabilize the LO frequency to the atomic reference transition at the clock frequency.

To analyze the impact of the laser FM noise on the short-term clock instability, we studied clock operation using the optical pumping laser frequency stabilized to two different reference transitions, labeled L1 and L2, obtained from the FRU or the reference module integrated in the LH. These reference transitions show a substantial difference in the FM-to-AM conversion factors through the local slope of absorption spectrum of the clock PP cell. As shown in Fig. 2, L1 corresponds to the crossover transition $|5S_{1/2}, F = 1\rangle \leftrightarrow |5P_{3/2}, F = 0, 1\rangle$ with an FM-to-AM conversion factor expressed in terms of photodetector current of 0.38 ± 0.03 nA/MHz, and L2 to the direct transition $|5S_{1/2}, F = 1\rangle \leftrightarrow |5P_{3/2}, F = 2\rangle$ with a nearly eight times higher conversion factor of 2.99 ± 0.06 nA/MHz. For the same experimental conditions (cell temperature, C-field, optical power, and microwave power), the change of the optical pump frequency is expected to have a direct impact on the short-term clock instability due to the laser FM noise via the FM-to-AM conversion phenomenon in the PP cell.

3. LASER NOISE CONTRIBUTION TO THE SHORT-TERM CLOCK INSTABILITY

In passive Rb atomic clocks, the main instability contributions in short timescales generally arise from the laser noises and the LO phase noise. The laser AM and FM noises affect the clock stability through two independent and distinct processes: the

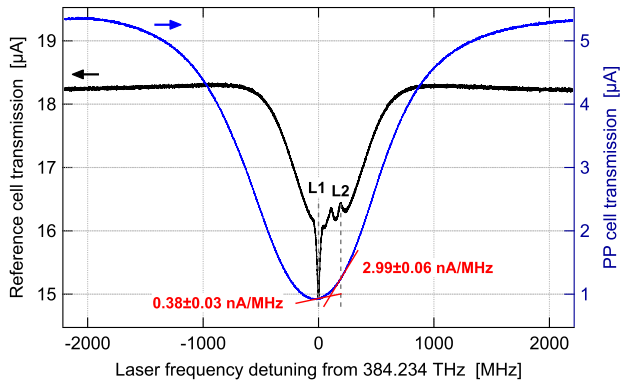

Fig. 2. Doppler-free absorption spectrum of the reference cell (left axis) and the linear transmission spectrum of the PP cell (right axis) measured using the LH. The two optical pump frequencies, L1 and L2, on the reference cell signal as well as the corresponding FM-to-AM conversion factors through the PP cell are indicated.

detection signal-to-noise ratio and the light-shift (LS) effects. In this section, we first discuss the clock's stability limit arising from the signal-to-noise ratio of the clock signal (S/N limit, see Section 3.A.3) as determined from the clock DR signal and noise both detected in the clock setup (cf. Fig. 1). Second, we evaluate the instability contributions of the laser intrinsic AM and FM noises, both measured at the output of the laser stabilization setup in Fig. 1, via the intensity and frequency LS effects, respectively. Finally, we present the total short-term clock instability estimations including all the different contributions.

A. Signal-to-Noise Limit

The S/N limited clock instability at 1 s can be estimated by [12]

$$\sigma_{S/N}(\tau) = \frac{N_{PSD}}{\sqrt{2} \cdot D_e \cdot \upsilon_{Rb}} \cdot \tau^{-1/2}, \qquad (1)$$

where N_{PSD} is the detection noise power spectral density (PSD), and D_e is the discriminator slope estimated using the DR signal parameters [$\approx 2 \cdot$ Amplitude/full width at half maximum (FWHM)]. The detection noise depends significantly on the intrinsic characteristics of the optical source and on its stabilization scheme. Therefore, it depends on the employed laser source. In contrast, the choice of the laser system has no significant impact on the other relevant DR signal parameters (amplitude, FWHM, and background signal) for identical experimental conditions (cell temperature, C-field, microwave power, and optical power).

We optimized the DR signal as a function of the optical power, the microwave power, and the microwave lock-in settings to reach the best clock S/N stability. For all the experiments presented in the following sections, the optical power at the PP input was 68.5 ± 1.5 μW. It was approximately 1 μW higher when using the LH instead of the frequency-doubled 1.56-μm source due to the discrete neutral-density filters employed. The microwave power was set to −36.4 dBm with a frequency-modulation frequency of 70 Hz and excursion of ±70 Hz.

1. DR Signals

The optimized DR signal parameters are gathered in Table 1. The amplitude, FWHM, discriminator, and contrast (ratio of the signal amplitude to the background dc level) are deduced from Lorentzian fits of the DR signal, and the frequency shift of the resonance center from the unperturbed Rb hyperfine splitting frequency is derived from the zero crossing of the demodulated error signal. The DR and the corresponding error signals are shown in Figs. 3(a) and 3(c), respectively, for optical pump frequency L1 and in Figs. 3(b) and 3(d) for L2. As it can be seen, the DR signal parameters do not depend on the employed laser. The amplitudes of the signal are the same, within error bars, in the four configurations studied. The difference in the optical power with individual lasers leads to slightly different DR signal line broadenings. For the optical pump frequency L1, higher contrasts are reached thanks to higher optical absorption in the PP cell compared to the absorption at L2. The central frequencies (ν_{cen}) of the DR signals are slightly shifted between the two optical pump frequencies due to the frequency light-shift effect with the coefficient of $7.2 \cdot 10^{-12}$/MHz (cf. Section 3.B).

2. Optical Detection Noise

The optical detection noise PSD on the atomic clock's photodetector at the microwave frequency-modulation frequency of 70 Hz is measured using a fast Fourier transform (FFT) spectrum analyzer. In Fig. 4(a) the typical N_{PSD} in the spectral region around the microwave modulation frequency are shown for the optical pump frequency L1 and in Fig. 4(b) for L2. The separate noise contributions of the lasers' AM and FM noises are estimated from these total optical detection noise measurements, taking into account the FM-to-AM conversion factors for L1 and L2. The AM noise of the laser sources is the dominant contribution to the clock's detection noise for laser frequencies near L1, for which the FM-to-AM noise conversion

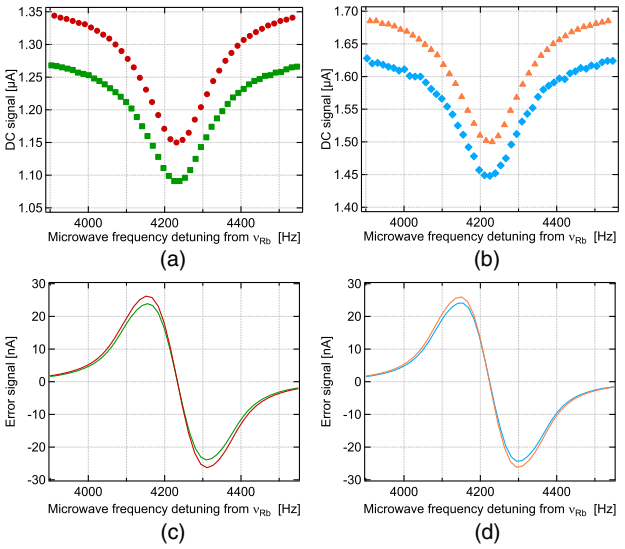

Fig. 3. DR signals measured for the optical pump frequency L1 in (a) using LH in green squares, using 1.56 μm-LD in red circles, and for L2 in (b) using LH in blue diamonds, using 1.56 μm-LD in orange triangles. The demodulated error signals in (c) for the optical pump frequency L1 and in (d) for L2 using the same color code as in (a) and (b).

Table 1. DR Signal Parameters for the Two Optical Pump Frequencies (L1 and L2) and the Two Lasers (LH and 1.56 µm-LD)

	Optical Pump Frequency L1		Optical Pump Frequency L2	
Signal Parameter	**LH**	**1.56 µm-LD**	**LH**	**1.56 µm-LD**
Amplitude [µA]	0.20 ± 0.01	0.21 ± 0.01	0.19 ± 0.01	0.21 ± 0.01
FWHM [Hz]	210.2 ± 0.8	212.2 ± 0.7	199.0 ± 1.9	203.6 ± 0.8
D_e [nA/Hz]	2.22 ± 0.01	2.42 ± 0.01	2.33 ± 0.03	2.43 ± 0.01
Contrast [%]	15.1 ± 0.1	15.7 ± 0.1	11.8 ± 0.1	12.1 ± 0.1
$(\nu_{cen} - \nu_{Rb})$ [Hz]	4233.3 ± 0.1	4233.5 ± 0.1	4224.4 ± 0.1	4223.6 ± 0.1

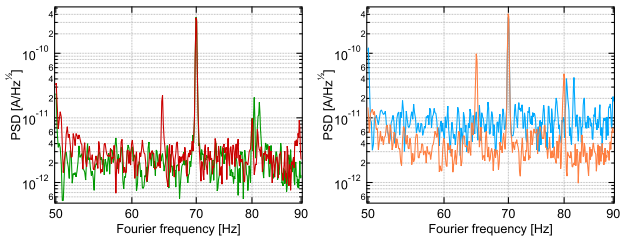

Fig. 4. Detection noise PSDs measured on the atomic clock setup's photodetector around the microwave modulation frequency of 70 Hz for the optical pump frequency L1 in (a) using LH in green, using 1.56 µm-LD in red, and for L2 in (b) using LH in blue, using 1.56 µm-LD in orange.

factor of the clock PP cell is lower. The noise contribution due to the FM-to-AM conversion through the clock PP cell becomes dominant for laser frequencies near L2. Nevertheless, for the 1.56 µm-LD compared to the LH, the contribution of this noise conversion phenomenon is reduced by more than a factor of two. In fact, thanks to the lower FM noise of the frequency-doubled telecom laser, the choice of the optical pump frequency has only a weak impact on the optical detection noise level of the clock operated with this laser rather than with the 780-nm LH.

3. Clock Instability Budget

The noise budgets of the S/N limited clock instability are given in Table 2 for the two optical pump frequencies using the two laser systems. The shot-noise limit is calculated for the photocurrent, I_{dc}, at the FWHM of the DR signal with the shot-noise $N_{\text{shot-noise}} = \sqrt{2 \cdot e \cdot I_{dc}}$, where e is the electron charge. The laser AM noise is the dominant S/N limiting factor for the optical pump frequency L1 using both lasers, due to the small FM-to-AM conversion factor found here. Thus, the estimated S/N limits for both lasers are similar and close to $1 \cdot 10^{-13}$. On the contrary, for L2, the detection noise contribution of the FM-to-AM noise conversion is the main limiting factor for both lasers. However, in the case of the 1.56 µm-LD, the FM noise contribution is two times lower than with the LH, leading to a better S/N limit for short-term clock instability.

B. Light-Shift Effects

In the CW-DR scheme, the laser light interaction with the atoms induces a shift of the atomic energy levels called the ac Stark effect [20], which directly results in a change of the clock frequency. The ac Stark shift, also known as the light shift (LS), depends on the optical spectrum of the light source, which means, in the case of a monochromatic laser source, on its intensity and wavelength. The clock frequency (ν_{clock}) shift caused by laser intensity fluctuations may be referred to as "intensity LS," and the shift caused by laser frequency fluctuations as "frequency LS." The clock frequency sensitivity to the laser light intensity (I_{laser}) fluctuations for a fixed laser frequency (ν_{laser}) is defined as the intensity LS coefficient: $\alpha = d\nu_{\text{clock}}/dI_{\text{laser}}$. The frequency LS coefficient β is defined as the clock frequency sensitivity to the laser frequency fluctuations for a fixed laser intensity: $\beta = d\nu_{\text{clock}}/d\nu_{\text{laser}}$. For the two optical pump frequencies L1 and L2 studied here, the β coefficient does not vary.

Table 2. Budget for the Clock's Signal-to-Noise Limit for the Two Optical Pump Frequencies (L1 and L2) and the Two Lasers (LH and 1.56 µm-LD)

	Optical Pump Frequency L1				Optical Pump Frequency L2			
	LH		1.56 µm-LD		LH		1.56 µm-LD	
Instability Source	N_{PSD} [pA · Hz$^{-1/2}$]	Predicted $\sigma(\tau) \cdot \tau^{-1/2}$	N_{PSD} [pA · Hz$^{-1/2}$]	Predicted $\sigma(\tau) \cdot \tau^{-1/2}$	N_{PSD} [pA · Hz$^{-1/2}$]	Predicted $\sigma(\tau) \cdot \tau^{-1/2}$	N_{PSD} [pA · Hz$^{-1/2}$]	Predicted $\sigma(\tau) \cdot \tau^{-1/2}$
Detector in the dark	0.2		0.2		0.2		0.2	
Shot-noise	0.6	$2.9 \cdot 10^{-14}$	0.6	$2.7 \cdot 10^{-14}$	0.7	$3.1 \cdot 10^{-14}$	0.7	$3.1 \cdot 10^{-14}$
Laser AM noise	2.1	$9.6 \cdot 10^{-14}$	2.9	$1.2 \cdot 10^{-13}$	2.1	$9.2 \cdot 10^{-14}$	2.9	$1.2 \cdot 10^{-13}$
Laser FM-to-AM noise conversion	1.3	$5.8 \cdot 10^{-14}$	0.6	$2.5 \cdot 10^{-14}$	9.8	$4.3 \cdot 10^{-13}$	4.6	$2.0 \cdot 10^{-13}$
Total S/N limit $\sigma_{S/N}(\tau)$	2.5	$1.2 \cdot 10^{-13}$	3.0	$1.3 \cdot 10^{-13}$	10.0	$4.4 \cdot 10^{-13}$	5.5	$2.3 \cdot 10^{-13}$

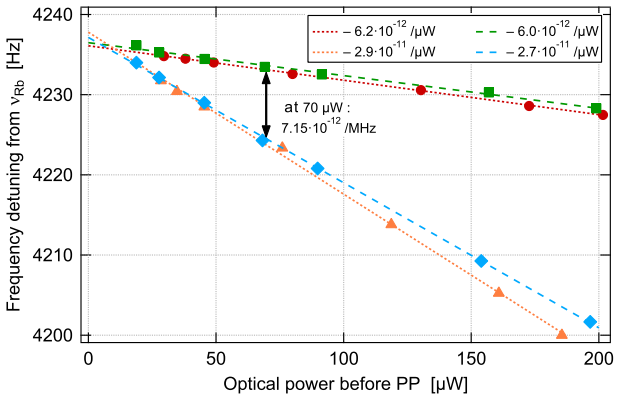

Fig. 5. Clock frequency shifts with respect to the unperturbed Rb ground-state hyperfine splitting energy as a function of the incident optical power. For the optical pump frequency L1, green squares: using LH, red circles: using 1.56 μm-LD. For the optical pump frequency L2, blue diamonds: using LH, orange triangles: using 1.56 μm-LD.

In Fig. 5, the clock frequency detuning from the unperturbed Rb hyperfine splitting frequency is plotted as a function of the optical power for the two laser frequencies L1 and L2 measured using both laser systems. Under same experimental conditions, the type of laser source has no significant impact on both LS coefficients. The α coefficients for each laser frequency, determined with a linear fit to the measured clock frequencies, are given in the inset. For the optical pump frequency L2, the intensity LS effect is larger than for L1 by more than a factor of four. Considering the detuning between the two optical pump frequencies L1 and L2 (193′053′600 Hz), the frequency LS coefficient β is determined as the measured clock frequency detuning for the known laser frequency detuning between L1 and L2. The β coefficient increases linearly for higher optical pump power. In our case, for an optical power of 70 μW, the frequency LS coefficient β is measured as $7.2 \cdot 10^{-12}$/MHz.

The intensity and frequency LS effects impact the clock instability at all timescales. In the short timescales, the relative intensity noise (RIN) and the FM noise of the laser are converted to clock frequency fluctuations through the LS effects with the corresponding coefficients α and β [21]. The RIN and FM noise, which are intrinsic to the laser [18] and depend largely on the laser operating conditions, are in the present case measured for LH at the level of 10^{-11} Hz^{-1} and 10^{8} Hz^{2}/Hz, respectively, and for 1.56 μm-LD, 10^{-10} Hz^{-1} and 10^{7} Hz^{2}/Hz. Note that in contrast to the DR signal noise (cf. Section 3.A.2) these laser noises are measured at the output of the laser stabilization setup (cf. Fig. 1). As it can be seen in Table 3, the clock instability contributions of the laser RIN and FM noise through the LS effects (σ_{α_LS} and σ_{β_LS}) are well below $1 \cdot 10^{-13}$ for 1 s of averaging time, which is lower than the limit due to the detection S/N discussed in the previous section.

On the longer timescales, the laser frequency and intensity fluctuations are also directly translated into clock frequency fluctuations through the LS effects. The impact of LS on the clock performance in the long term is not addressed in this paper; preliminary predictions concerning the two lasers evaluated here are given in Ref. [18] for the case of our Rb clock operated in the pulsed optically pumped (POP) scheme [22].

C. Total Short-Term Clock Instability Estimations

In addition to the clock frequency instability contributions from the laser noises, the LO phase noise, through the intermodulation effects [23], can also be an important instability source in the short timescales. In our case, for a modulation frequency of 70 Hz, the calculated contribution of the LO phase noise is $\sigma_{LO} = 1.6 \cdot 10^{-13} \cdot \tau^{-1/2}$, taking into account the even harmonics of 70 Hz up to 10 kHz. Compared to the impact of the laser noise, this contribution is slightly higher than the short-term clock instability for the laser frequency L1 and thus one of the two dominant limiting factors in these cases. As for L2, while the LO phase noise contribution remains important, the short-term clock instability is limited by the S/N, mostly due to the FM-to-AM noise conversion phenomenon. The LO phase noise contribution can be reduced for lower microwave modulation frequencies, though at the expense of higher optical detection noise at lower frequencies. In our case, the modulation frequency is chosen with the trade-off between the LO phase noise and the optical detection noise.

Individual instability contributions of the laser and LO noises are gathered in Table 3. The total short-term clock instability squared, $(\sigma_y)^2$, is estimated by summing the squares of each contribution as in the following expression [14]:

$$\sigma_y = \sqrt{\sigma_{S/N}^2 + \sigma_{\alpha\_LS}^2 + \sigma_{\beta\_LS}^2 + \sigma_{LO}^2}. \quad (2)$$

4. CLOCK INSTABILITY MEASUREMENTS

The clock frequency instabilities measured with the two lasers are shown in Figs. 6(a) and 6(b) for optical pump frequencies L1 and L2, respectively. In good agreement with

Table 3. Estimated Total Short-Term Clock Instabilities for the Two Optical Pump Frequencies (L1 and L2) and the Two Lasers (LH and 1.56 μm-LD)

	Optical Pump Frequency L1		Optical Pump Frequency L2	
(τ = 1s)	LH	1.56 μm-LD	LH	1.56 μm-LD
$\sigma_{S/N}(\tau)$	$1.2 \cdot 10^{-13}$	$1.3 \cdot 10^{-13}$	$4.4 \cdot 10^{-13}$	$2.3 \cdot 10^{-13}$
$\sigma_{\alpha\_LS}(\tau)$	$1.2 \cdot 10^{-15}$	$3.6 \cdot 10^{-15}$	$5.5 \cdot 10^{-15}$	$1.7 \cdot 10^{-14}$
$\sigma_{\beta\_LS}(\tau)$	$7.2 \cdot 10^{-14}$	$2.3 \cdot 10^{-14}$	$7.2 \cdot 10^{-14}$	$2.3 \cdot 10^{-14}$
$\sigma_{LO}(\tau)$	$1.6 \cdot 10^{-13}$	$1.6 \cdot 10^{-13}$	$1.6 \cdot 10^{-13}$	$1.6 \cdot 10^{-13}$
Estimated $\sigma_y(\tau)$	$2.1 \cdot 10^{-13}$	$2.1 \cdot 10^{-13}$	$4.8 \cdot 10^{-13}$	$2.9 \cdot 10^{-13}$
Measured $\sigma_y(\tau)$	$2.3 \cdot 10^{-13}$	$2.4 \cdot 10^{-13}$	$8.8 \cdot 10^{-13}$	$3.1 \cdot 10^{-13}$

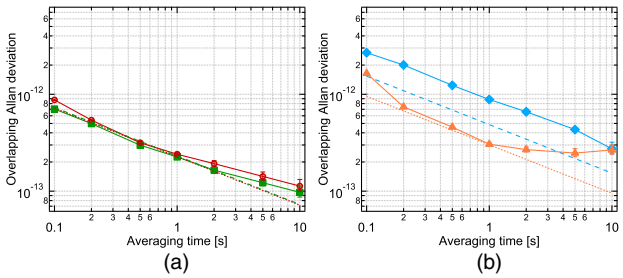

Fig. 6. Clock frequency instabilities measured for optical pump frequency L1 in (a) using LH in green squares, using 1.56 μm-LD in red circles, and for L2 in (b) using LH in blue diamonds, using 1.56 μm-LD in orange triangles. The short-term estimations are indicated in dashed lines for LH and dotted lines for 1.56 μm-LD, in the same color as the corresponding measurement.

the predictions, the short-term clock instabilities using both lasers for the optical pumping at L1 are at a similar level below $2.5 \cdot 10^{-13} \cdot \tau^{-1/2}$. As for the optical pump frequency L2, the instability contribution of the FM noise conversion is one order of magnitude higher for both lasers and becomes the dominant limiting factor in the short-term clock instability. For the 1.56 μm-LD, the choice of the optical pump frequency has little impact on the clock performance thanks to its low FM noise. In our case, the measured short-term clock instability is improved by a factor of three for the low-noise 1.56 μm-LD as compared to the LH. The measured clock instability is slightly higher than our estimations for the LH used for optical pumping at L2.

At averaging time of 10 s, the clock instabilities are degraded due to the optical power fluctuations at the PP input via the intensity LS effect. The PM fiber connection between the two parts of the setup does not introduce significant additional power fluctuations at longer timescales up to 100 s due to the thermal and mechanical isolation employed. The optical power fluctuations are mainly due to the etalon effects in the fibered paths, and the impact via the intensity LS depends on the α coefficient for the given experimental conditions (laser frequency, cell temperature, etc.). Thus, the impact of the intensity LS may be reduced not only by decreasing the optical power fluctuations but also with a rigorous choice of the experimental conditions minimizing the α coefficient. Also, the alternative clock operation schemes, such as POP [22], for which the light and microwave interactions are separated in time, may significantly reduce the LS effects as the light and microwave interactions are separated in time.

For timescales around 10 s, the relative optical power fluctuations are larger by one order of magnitude for the fibered 1.56 μm-LD as compared to the free-space LH [18]. The measured power fluctuations at 10 s create clock frequency fluctuations on the level of $\approx 7.5 \cdot 10^{-14}$ for the optical pump frequency L1 using the 1.56 μm-LD and $\approx 3.5 \cdot 10^{-13}$ for L2. This latter limit is more pronounced than for L1 owing to the higher α coefficient measured for the optical pump frequency L2 (cf. Fig. 5) and in good agreement with the measured clock instability for this laser shown in Fig. 6(b). For the free-space LH, the clock instability contribution due to the optical power fluctuations at 10 s is negligible at both optical pump frequencies studied ($< 3 \cdot 10^{-14}$ for the optical pump frequency L2, $< 7 \cdot 10^{-15}$ for L1).

5. CONCLUSION

We have evaluated the application of a frequency-doubled 1.56-μm telecom laser as the pump light source in a high-performance Rb vapor-cell atomic clock. A short-term frequency instability better than $2.5 \cdot 10^{-13} \cdot \tau^{-1/2}$ has been demonstrated, which is comparable to other state-of-the-art clock schemes based on laser diodes emitting at the Rb or Cs optical pump wavelength [14,24]. Hence, the frequency-doubled telecom laser allows at least as good clock frequency stability as the 780-nm laser, while being based on high-reliability telecom components, which is of high relevance for real-world applications of Rb atomic clocks.

We analyzed in detail the impact of the laser AM and FM noises on the clock performance. We showed that, thanks to the low FM noise level of the telecom laser, the short-term stability of the clock using this laser is only weakly impacted by the choice of the optical pump frequency and thus by the FM-to-AM noise conversion occurring in the Rb vapor cell of the clock PP. For laser frequencies inducing a non-optimal high FM-to-AM noise conversion factor through the PP cell, the short-term clock stability is improved by nearly a factor of three using a low-noise telecom laser, whereas for laser frequencies corresponding to a low FM-to-AM conversion factor, besides the technical limitation due to the employed LO, the dominant contributions in the short timescales are the lasers' AM noise. For longer timescales, the slower optical intensity fluctuations arising from the etalon effects in the fiber-pigtailed laser system [18] grow in importance and can impact the clock performance through the intensity light-shift effect.

Funding. Schweizerischer Nationalfonds zur Förderung der Wissenschaftlichen Forschung (SNF) (156621, 162346).

Acknowledgment. We thank our colleague Mohammadreza Gharavipour for his previous contributions concerning the cavity, and Patrick Scherler and Marc Durrenberger for their technical support.

REFERENCES

1. M. Ohtsu and E. Ikegami, "Frequency stabilisation of 1.5 μm DFB laser using internal second harmonic generation and atomic ^{87}Rb line," Electron. Lett. **25**, 22–23 (1989).
2. M. Poulin, N. Cyr, C. Latrasse, and M. Tetu, "Progress in the realization of a frequency standard at 192.1 THz (1560.5 nm) using ^{87}Rb D_2-line and second harmonic generation," IEEE Trans. Instrum. Meas. **46**, 157–161 (1997).
3. Y. Han, S. Guo, J. Wang, H. Liu, J. He, and J. Wang, "Efficient frequency doubling of a telecom 1560 nm laser in a waveguide and frequency stabilization to Rb D2 line," Chin. Opt. Lett. **12**, 121401 (2014).
4. R. J. Thompson, M. Tu, D. C. Aveline, N. Lundblad, and L. Maleki, "High power single frequency 780 nm laser source generated from frequency doubling of a seeded fiber amplifier in a cascade of PPLN crystals," Opt. Express **11**, 1709–1713 (2003).
5. H. C. Chui, Y. W. Liu, J. T. Shy, S. Y. Shaw, R. V. Roussev, and M. M. Fejer, "Frequency-stabilized 1520-nm diode laser with rubidium $5S_{1/2} \rightarrow 7S_{1/2}$ two-photon absorption," Appl. Opt. **43**, 6348–6351 (2004).

6. S. Peil, S. Crane, T. Swanson, and C. R. Ekstrom, "The USNO rubidium fountain," in *Proceedings of IEEE International Frequency Control Symposium and Exposition* (IEEE, 2006), pp. 304–306.
7. T. Lévèque, L. Antoni-Micollier, B. Faure, and J. Berthon, "A laser setup for rubidium cooling dedicated to space applications," Appl. Phys. B **116**, 997–1004 (2014).
8. F. Theron, Y. Bidel, E. Dieu, N. Zahzam, M. Cadoret, and A. Bresson, "Frequency-doubled telecom fiber laser for a cold atom interferometer using optical lattices," Opt. Commun. **393**, 152–155 (2017).
9. J. Camparo, "The rubidium atomic clock and basic research," Phys. Today **60**(11), 33–39 (2007).
10. J. Vanier and C. Mandache, "The passive optically pumped Rb frequency standard: the laser approach," Appl. Phys. B **87**, 565–593 (2007).
11. C. E. Wieman and L. Hollberg, "Using diode lasers for atomic physics," Rev. Sci. Instrum. **62**, 1–20 (1991).
12. G. Mileti and P. Thomann, "Study of the S/N performance of passive atomic clocks using a laser pumped vapour," in *Proceedings of European Frequency and Time Forum* (1995), pp. 271–276.
13. J. C. Camparo, "Conversion of laser phase noise to amplitude noise in an optically thick vapor," J. Opt. Soc. Am. B **15**, 1177–1186 (1998).
14. T. Bandi, C. Affolderbach, C. Stefanucci, F. Merli, A. K. Skrivervik, and G. Mileti, "Compact, high-performance CW double-resonance rubidium Standard with $1.4 \times 10^{-13}\ \tau^{-1/2}$ stability," IEEE Trans. Ultrason. Ferroelectr. Freq. Control **61**, 1769–1778 (2014).
15. F. Gruet, M. Pellaton, C. Affolderbach, T. Bandi, R. Matthey, and G. Mileti, "Compact and frequency stabilized laser heads for Rubidium atomic clocks," Proc. SPIE **10564**, 105642Y (2017).
16. M. Pellaton, C. Affolderbach, Y. Pétremand, N. de Rooij, and G. Mileti, "Study of laser-pumped double-resonance clock signals using a microfabricated cell," Phys. Scripta **T149**, 014013 (2012).
17. R. Matthey, F. Gruet, S. Schilt, and G. Mileti, "Compact rubidium-stabilized multi-frequency reference source in the 1.55-μm region," Opt. Lett. **40**, 2576–2579 (2015).
18. N. Almat, W. Moreno, M. Pellaton, F. Gruet, C. Affolderbach, and G. Mileti, "Characterization of frequency-doubled 1.5-μm lasers for high-performance Rb clocks," IEEE Trans. Ultrason. Ferroelectr. Freq. Control (to be published).
19. C. Stefanucci, T. Bandi, F. Merli, M. Pellaton, C. Affolderbach, G. Mileti, and A. K. Skrivervik, "Compact microwave cavity for high performance rubidium frequency standards," Rev. Sci. Instrum. **83**, 104706 (2012).
20. B. S. Mathur, H. Tang, and W. Happer, "Light shifts in the alkali atoms," Phys. Rev. **171**, 11–19 (1968).
21. J. Vanier and C. Tomescu, *The Quantum Physics of Atomic Frequency Standards: Recent Developments* (CRC Press, 2016), pp. 287–295.
22. S. Micalizio, C. E. Calosso, A. Godone, and F. Levi, "Metrological characterization of the pulsed Rb clock with optical detection," Metrologia **49**, 425–436 (2012).
23. J. Q. Deng, G. Mileti, R. E. Drullinger, D. A. Jennings, and F. L. Walls, "Noise considerations for locking to the center of a Lorentzian line," Phys. Rev. A **59**, 773–777 (1999).
24. M. Abdel Hafiz, G. Coget, P. Yun, S. Guérandel, E. de Clercq, and R. Boudot, "A high-performance Raman-Ramsey Cs vapor cell atomic clock," J. Appl. Phys. **121**, 104903 (2017).